



One-Pot Self-Assembly of Sequence-Controlled Mesoporous Heterostructures via **Structure-Directing Agents**

Taylor Larison, Eric R. Williams, Mason Wright, Mengxue Zhang, John Tengco, Matthew G. Boebinger, Chuanbing Tang, and Morgan Stefik*



Downloaded via UNIV MONTPELLIER on August 6, 2024 at 17:38:50 (UTC). See https://pubs.acs.org/sharingguidelines for options on how to legitimately share published articles.

Cite This: ACS Nano 2024, 18, 20133-20141



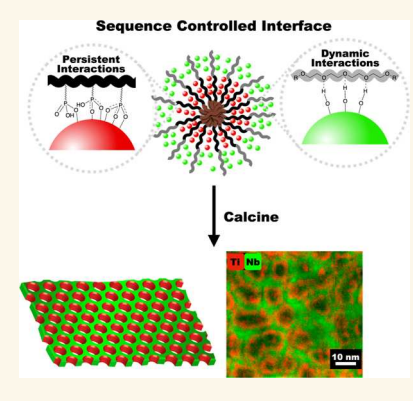
ACCESS I

Metrics & More

Article Recommendations

Supporting Information

ABSTRACT: Multimaterial heterostructures have led to characteristics surpassing the individual components. Nature controls the architecture and placement of multiple materials through biomineralization of nanoparticles (NPs); however, synthetic heterostructure formation remains limited and generally departs from the elegance of self-assembly. Here, a class of block polymer structure-directing agents (SDAs) are developed containing repeat units capable of persistent (covalent) NP interactions that enable the direct fabrication of nanoscale porous heterostructures, where a single material is localized at the pore surface as a continuous layer. This SDA binding motif (design rule 1) enables sequence-controlled heterostructures, where the composition profile and interfaces correspond to the synthetic addition order. This approach is generalized with 5 material sequences using an SDA with only persistent SDA-NP interactions ("P-NP₁-NP₂"; NP₁ = TiO₂, Nb₂O₅, ZrO₂). Expanding these polymer SDA design guidelines, it is shown that the combination of both persistent and dynamic



(noncovalent) SDA-NP interactions ("PD-NP₁-NP₂") improves the production of uniform interconnected porosity (design rule 2). The resulting competitive binding between two segments of the SDA (P- vs D-) requires additional time for the first NP type (NP₁) to reach and covalently attach to the SDA (design rule 3). The combination of these three design rules enables the direct self-assembly of heterostructures that localize a single material at the pore surface while preserving continuous porosity.

KEYWORDS: mesoporous, heterostructure, self-assembly, phosphonic acid, sequence control

oing beyond the characteristics of individual materials, composites and heterojunctions often enable enhanced capabilities with controlled material sequences. ¹⁻⁴ Many such applications also require porous materials, e.g., solar cells, ⁵⁻⁷ rechargeable batteries, ⁸⁻¹⁰ supercapacitors, ¹¹⁻¹⁴ fuel cells, ^{15,16} and tandem catalysts. ¹⁷ Nature has adapted the ability to regulate the composition and architecture of inorganic materials using nanoparticle (NP) self-assembly through biomineralization to create mechanically advantageous inorganic-organic composite structures with elegant control. 19 In contrast, inorganic-inorganic heterostructures, e.g., topological electronic materials, ²⁰ optoelectronics, ²¹ or tandem catalysts, do not have natural analogs.^{20,22,23} Heterostructure synthesis generally requires extended multistep processes. For example, top-down approaches use lithography with sequential depositions and depart from the elegance of self-assembly. Bottom-up approaches generally start from a single porous material, which is subsequently coated by chemical vapor deposition, atomic layer deposition, or layer-by-layer deposition, which

require multiple steps and are difficult to adapt to different compositions. Some bottom-up approaches have included covalent attachment of nanoparticles to structure-directing agents (SDAs), however, e.g., DNA origami remains limited to solution/surface structures.²⁴ Simple one-pot self-assembly approaches would significantly improve the generalized synthesis of continuous and freestanding heterostructures.

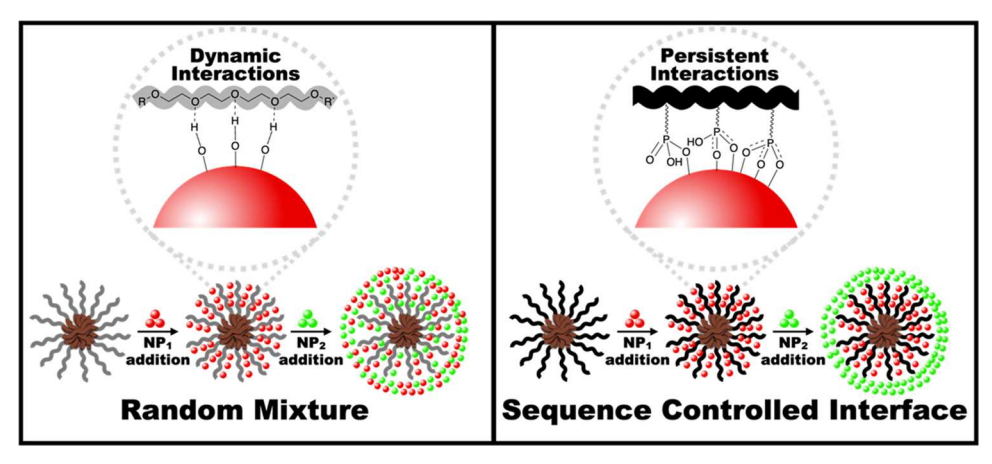
Block polymer SDAs self-assemble with NP material precursors for facile and cost-effective control over the formation of individual porous materials, such as silicates, ^{25,26} metal oxides, ^{27–34} carbons, ^{35–37} and metals, ^{38,39} with diverse architectures. Generally, the material precursors associate

Received: February 12, 2024 Revised: June 24, 2024 Accepted: June 25, 2024 Published: July 29, 2024





Scheme 1. Dynamic versus Persistent SDA-NP interactions^a



^aThe use of dynamic interactions with conventional polymer SDAs leads to random mixtures whenever multiple types of NPs are combined. In contrast, persistent interactions enable the saturation of phosphonic acid moieties with NP₁, followed by the peripheral assembly of NP₂, thus encoding the addition sequence in the resulting interfaces. Phosphonic acids have mono-, bi-, and tridentate binding capabilities to diverse NP chemistries for generalized sequence-controlled synthesis.

selectively with one hydrophilic polymer block via dynamic intermolecular interactions, such as hydrogen bonding or Coulombic interactions, while a second block phase separates, such that subsequent polymer removal yields porosity. While this is a popular strategy, when paired with multiple materials, the resulting composites are generally limited to random mixtures 40,41 due to the dynamic SDA-NP interactions (Scheme 1). Covalent attachment of NPs to polymer SDAs has remained limited to chain-end attachment thus far, which leads to isolated material patches rather than continuous layers. 42 Likewise, NP placement within SDAs has been controlled via the areal density of surface grafted polymer chains which can result in isolated material patches. 43-48 Alternatively, reports of sequential depositions of SDAs with different materials are not heterostructures in the same sense since the compositions do not vary on the length scale of the walls/pores. 492 So far, the SDA synthesis of continuous materials has generally utilized dynamic interactions, which continuously break and reform, thus erasing any history of the addition order.

Here, a class of SDAs are advanced that rather include repeat units with persistent SDA-NP interactions through covalent linkages. While SDA-NP interaction strengths and exchange kinetics vary over a continuum, we suggest that "persistent" attachment is a distinct condition when the energetics of SDA-NP separation are comparable with breakdown of the NP or the SDA.⁵⁰ Specifically, a repeated phosphonic acid motif is demonstrated to enable chemical attachment of the first added NP type (NP₁) to the SDA. Here, each NP composition is considered a different type since each is associated with different synthesis conditions and size distributions. The second NP type (NP₂) added then organizes around the periphery of NP₁, thus encoding the processing sequence in the resulting heterostructure (Scheme 1). Thus, a simple onepot process is reported for the direct self-assembly of heterostructures based on a generalized binding strategy that is compatible with diverse NP types. Two block polymers with persistent SDA-NP interactions were used as micelle templates, including an AB diblock polymer (samples P-NP₁-NP₂) and a bis-hydrophilic ABC triblock terpolymer containing a block with dynamic NP interactions and one with persistent NP

interactions (samples PD-NP₁-NP₂). The ABC strategy enabled the one-pot self-assembly of periodic mesoporous heterostructures.

RESULTS AND DISCUSSION

SDA Design Choices. Several candidate functional groups for SDA-NP interactions were considered for forming persistent linkages. For example, metal oxides interact with the following functional groups arranged in order of increasing interaction strength: ether, carboxylate, acetylacetonate, phosphonic acid, and silane. Here, higher-order multidentate interactions, such as phosphonic acids⁵¹ and silanes, naturally have higher interaction strengths; however, silanes are prone to homocondensation reactions. Phosphonic acid groups were selected since these are also compatible more broadly with binding metal chalcogenides,⁵³ metal/metal ions,^{54–56} and quantum dots.⁵⁷ The connection of this functional group to the polymer backbone is also important, where phosphonates (R-PO₃H₂) are more resistant to hydrolysis than phosphates (R-O-PO₃H₂). The phase-separating hydrophobic block has broader criteria, however, including a high $T_{\rm g}$ block can enable glassy core micelles that enable constant template size.⁵⁸ Thus, a poly(cyclohexyl methacrylate-b-methacryloyloxymethyl phosphonic acid) (PCHMA-b-PMMPA) was synthesized using reversible addition-fragmentation chain-transfer (RAFT) and postpolymerization reactions (Figure S1 and Table S1-S2).⁵⁸ This polymer combines a phosphonic acid containing a PMMPA block and a glassy PCHMA block for subsequent porosity. For comparison sake, poly(styrene-b-ethylene oxide) (PS-b-PEO) was synthesized using atom transfer radical polymerization, which combines the prototypical PEO block with NP interactions and a glassy, hydrophobic PS block.

SDA-NP Binding Experiments. The SDA-NP interactions for these two SDAs were examined with binding experiments. The first experiment examined the separation of SDAs from NPs. Here, an excess of acid-stabilized TiO₂ NPs were added to either PCHMA-b-PMMPA or PS-b-PEO micelles, where subsequent base addition induced NP aggregation and precipitation. The solutions were filtered to remove the NP precipitant, the solvent was evaporated, and any residue was dispersed in CDCl₃ for ¹H NMR measurement (Figure 1).

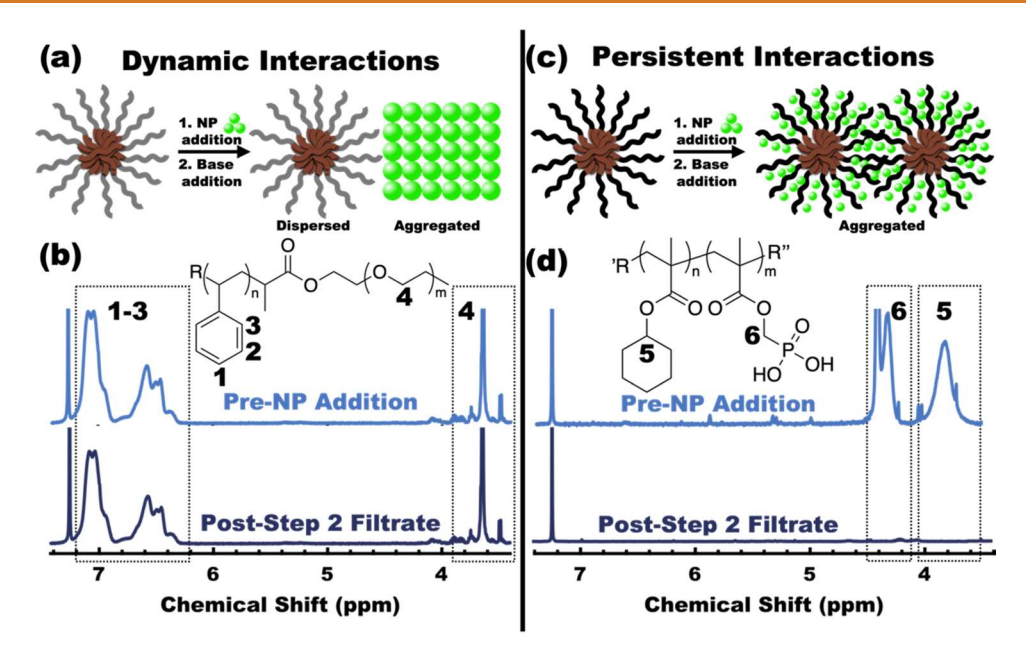


Figure 1. Dynamic vs persistent binding of TiO₂ NPs to different hydrophilic polymers was examined by filtering destabilized NPs (base addition) from polymer solutions. Here, (a) dynamic polymer–NP interactions lead to polymer release from NP aggregates, whereas (c) persistent interactions cause coaggregation. Hydrophilic blocks of (b) PEO and (d) PMMPA are compared with ¹H NMR patterns both "pre-NP addition" as references and "postfiltration." The PS-b-PEO found postfiltration confirms dynamic (reversible) PEO-NP interactions, whereas the lack of the PCHMA-b-PMMPA signal confirms persistent PMMPA-NP interactions. All NMR measurements were taken in CDCl₃ and data were offset vertically for clarity.

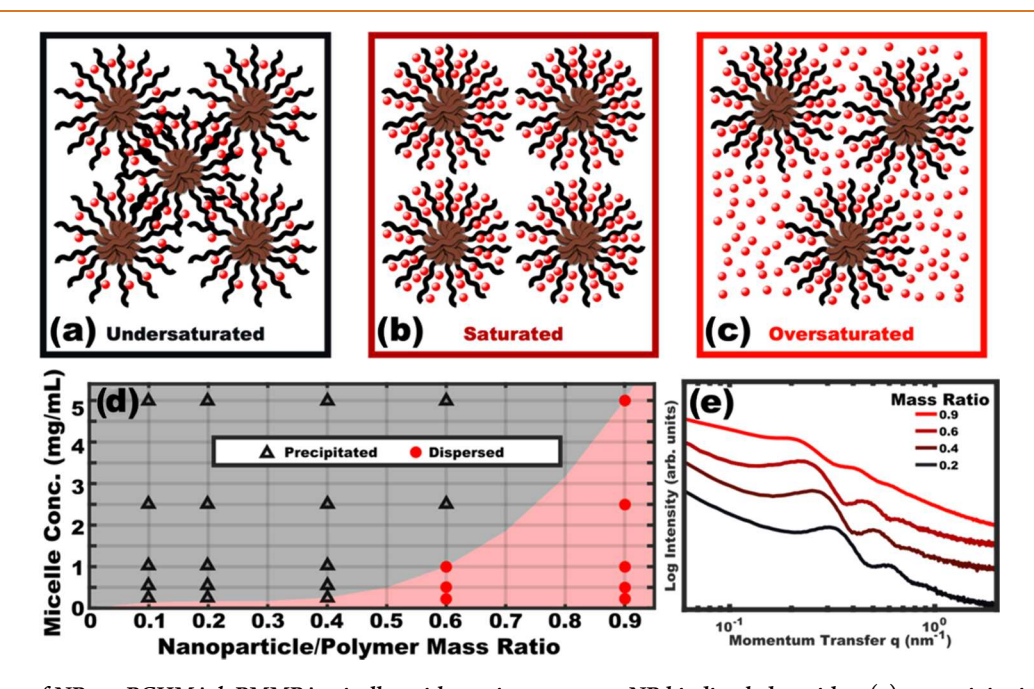


Figure 2. Addition of NPs to PCHMA-b-PMMPA micelles with persistent corona-NP binding led to either (a) coprecipitation or (b,c) stable dispersions (lighter reds) depending on the NP/SDA mass ratio. (d) The dispersion behavior was mapped as a function of proportions and concentration to show equilibrium and kinetic stability. The point of "saturation" was determined as the minimum NP loading for equilibrium stability. (e) SAXS after evaporative concentration revealed increasing micelle spacing with NP loading, where the structure factor peaks broadened upon oversaturation. SAXS data were offset vertically for clarity.

Thus, the observation of SDA in this final solution would identify whether or not it was anchored to the NPs. Comparison of ¹H NMR of the pure polymers to these filtrates revealed that PS-*b*-PEO was released from the NPs, whereas the absence of PCHMA-*b*-PMMPA indicated that it remained bound to the NPs. Separate control experiments without NPs confirmed that PCHMA-*b*-PMMPA remained in

solution after base addition, thus eliminating polymer solubility as an alternative explanation. These results demonstrate the dynamic PEO-NP interaction, whereas PMMPA remained persistently bonded to the NPs during condensation and precipitation. The second binding experiment examined dispersion stability with persistent SDA-NP interactions. The TiO_2 NPs used here as well as the Nb_2O_5 and ZrO_2 NPs used

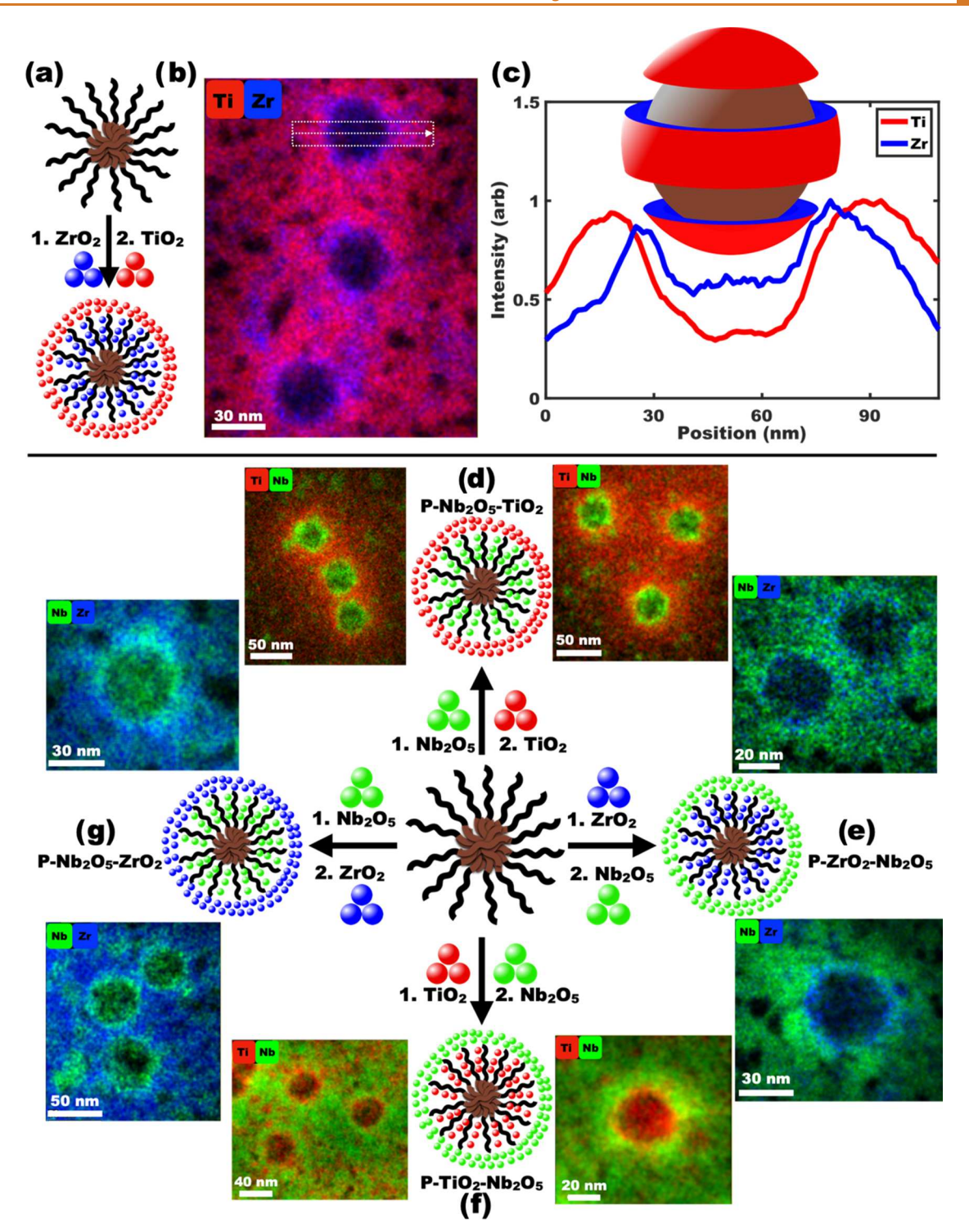


Figure 3. Sequence-controlled heterostructure synthesis is prepared using persistent SDA-NP interactions (PCHMA-b-PMMPA) with NP $_1$ = ZrO $_2$ and NP $_2$ = TiO $_2$ (a). Threshold-colorized STEM-EDS data is shown, where the synthetic sequences correspond to the composition sequences (b). A normalized compositional line scan shows the anticipated composition sequence (inset sketch) (c). Sequence-controlled heterostructure synthesis was then generalized using various combinations of Nb $_2$ O $_5$ (green), TiO $_2$ (red), and ZrO $_2$ (purple) (d-g). In each case, NP $_1$ saturated the PMMPA block (see Figure 2b), where NP $_2$ localized around the corona periphery (named P-NP $_1$ -NP $_2$). These data demonstrate the first design rule, where repeated covalent attachment points on the SDA enable continuous layers of NP $_1$.

later were all spherical with <5 nm dimensions (3.2 ± 0.8 , 3.9 ± 0.9 , and 4.5 ± 1.6 nm for TiO₂, Nb₂O₅, and ZrO₂) as determined by TEM (Figure S2, Table S3). When TiO₂ NPs were added to micelle solutions, it was observed that solutions with low ratios of NP/PCHMA-*b*-PMMPA led to precipitant formation. It is suggested that coaggregation occurs when

multiple micelles bind to the same NPs. ⁵⁰ Even small e.g. 2 nm diameter NPs have sufficient surface area (12.6 nm²) for \sim 40 binding sites given the small saturated surface area for phosphonic acids (\sim 0.3 nm²). This in combination with the flexible nature of solvated polymer chains could enable the formation of such extended networks that precipitate. In

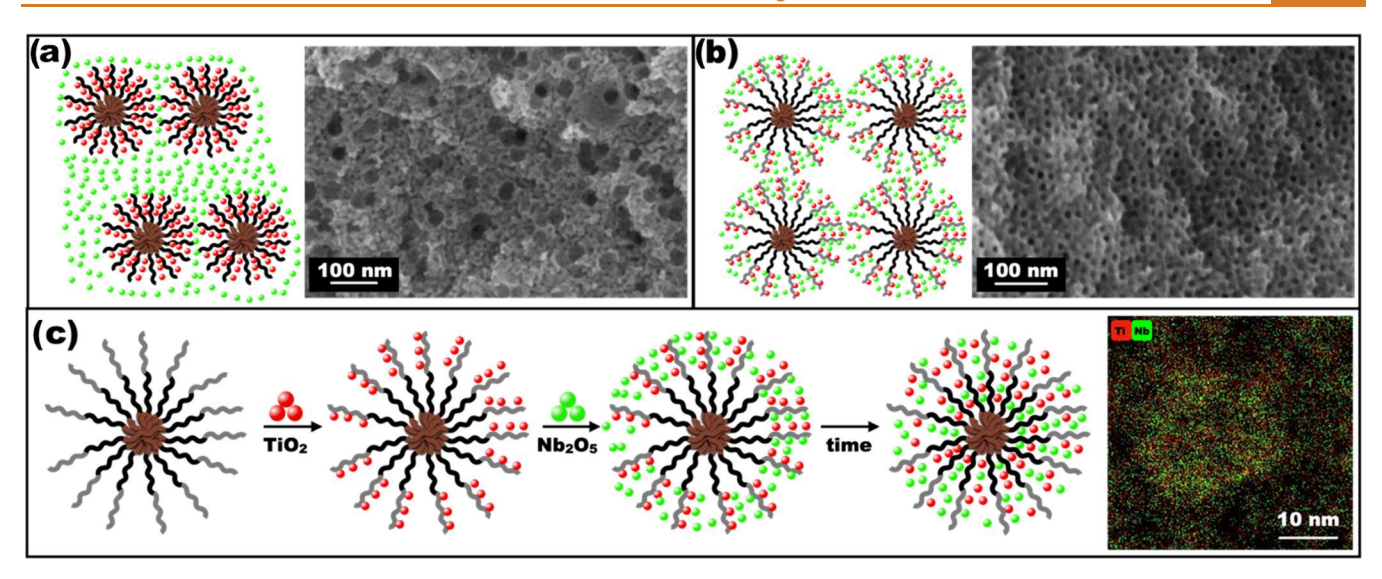


Figure 4. SEM images of porous materials from $P-TiO_2-Nb_2O_5$ exhibited disordered porosity that was attributed to the lack of a corona with dynamic NP interactions (a). The addition of a PEO-like terminal block (PCHMA-b-PMMPA-b-PPEGMA) enabled samples with uniform micelle spacing and continuous porosity (b), establishing the second design rule. Initial attempts at heterostructure synthesis, however, led to NP mixing as revealed by STEM-EDS composition maps. The NP mixing suggested a critical time to NP₁ to reach PMMPA (c), which led to the third design rule.

contrast, higher ratios led to stable dispersions of nonaggregated and NP-loaded micelles. This ratio and micelle concentrations were screened to map both kinetic stability (dilute micelles) and equilibrium stability ((super)saturated micelles) (Figure 2a-d). Here, the term "saturation" means sufficient NP loading to inhibit micelle-NP-micelle aggregation and does not imply that all phosphonic acid groups were reacted. The third binding experiment examined the structure of the dried SDA-NP assemblies by small-angle X-ray scattering (SAXS) after solvent removal. Here, the SAXS dspacing $(d = 2\pi/q)$ corresponds to the micelle-to-micelle spacing,⁵⁹ which increased with the addition of NPs, confirming the well-behaved self-assembly of the ensemble to yield periodic structures (Figure 2e). The dispersion stability correlated with the SAXS profiles, where supersaturation of the SDA with NPs led to a broadened structure factor, indicating less extent of ordering. The saturation ratios of NP/SDA were determined for all NP types examined (TiO₂, Nb₂O₅, ZrO₂) based on dispersion stability. Thus, the phosphonic acid containing a PMMPA block was shown to strongly bind to diverse NP types and influence both the SDA dispersion stability and self-assembly depending on if the NP loading reached the defined saturation condition.

Persistent Binding Repeat Units Enable Sequence-Controlled Heterostructure Synthesis. The ability to self-assemble heterostructures was examined by saturating PCHMA-b-PMMPA micelles with a first NP type (NP₁), followed by the addition of a second (NP₂). The compositions examined included NP_i = TiO_2 , Nb₂O₅, or ZrO_2 , where the composition and addition order were widely varied. Samples were termed "P-[NP₁]-[NP₂]" to reflect the persistent interactions and the NP addition order. Scanning transmission electron microscopy using energy-dispersive X-ray spectroscopy (STEM-EDS) yielded spatial composition maps. The images were presented using intensity thresholds since the 3D geometry of the micelle leads to regions of predominance for NP₁ and NP₂ signals while being non-zero at all locations. As a representative example, the results of P-ZrO₂-TiO₂ are

elaborated first (Figure 3a) where the resulting sequence of ZrO₂ (core) and TiO₂ (shell) heterostructure was consistent with the sequence of material additions (Figure 3b). Here, the localization of a 9.0 \pm 3.0 nm shell of ZrO₂ around the 27.8 \pm 3.0 nm micelle core was plainly visible within a continuous TiO₂ matrix. The corresponding normalized line scans (Figure 3c), show this position-dependent composition, where the TiO₂ content reduces at the onset of the ZrO₂ shell. Here, the carbon content is maximum across the micelle cores, consistent with the expectations (inset sketch). Four additional synthetic sequences were examined (Figure 3d-g), including $P-Nb_2O_5-TiO_2$, $P-TiO_2-Nb_2O_5$, $P-Nb_2O_5-ZrO_2$, and $P-Nb_2O_5-ZrO_2$ ZrO₂-Nb₂O₅, each starting from micelles saturated with NP₁ (Table S4). Please note that oversaturated micelles (Figure 2) would rather result in an abundance NP1 mixed in the NP2 matrix. Single-element images are also presented in Figure S3. Notably, all of these sequences exhibited similar heterostructure shell thicknesses of 8.2 \pm 1.8, 8.9 \pm 2.2, 8.8 \pm 2.8, and 8.6 ± 1.8 nm, respectively, consistent with the use of the same SDA for each. These examples demonstrate controlled sequence reversal, e.g., compare P-Nb₂O₅-TiO₂ to P-TiO₂-Nb₂O₅ or P-Nb₂O₅-ZrO₂ to P-ZrO₂-Nb₂O₅. Furthermore, a control experiment using the dynamic interactions of PS-b-PEO micelles (D-Nb₂O₅-TiO₂) resulted in a random mixture of the two oxides (Figure S4). These data sets demonstrate significant SDA design criteria, where a repeated motif with persistent interactions enables layered heterostructures, where the synthetic sequence is encoded in the resulting material sequence as demonstrated with diverse material compositions and reversible ordering.

Bis-Hydrophilic Triblock Terpolymer SDA Enables Ordered and Continuous Porosity. Porous structures were prepared using calcination (heat) to remove the SDAs. The materials resulting from PCHMA-b-PMMPA (P-NP₁-NP₂ samples) however exhibited nonuniform micelle-micelle spacings by SEM (Figure 4a), where clustering of micelle templates was apparent among an uneven distribution of NP₂. Such nonperiodic arrangements inhibit realization of con-

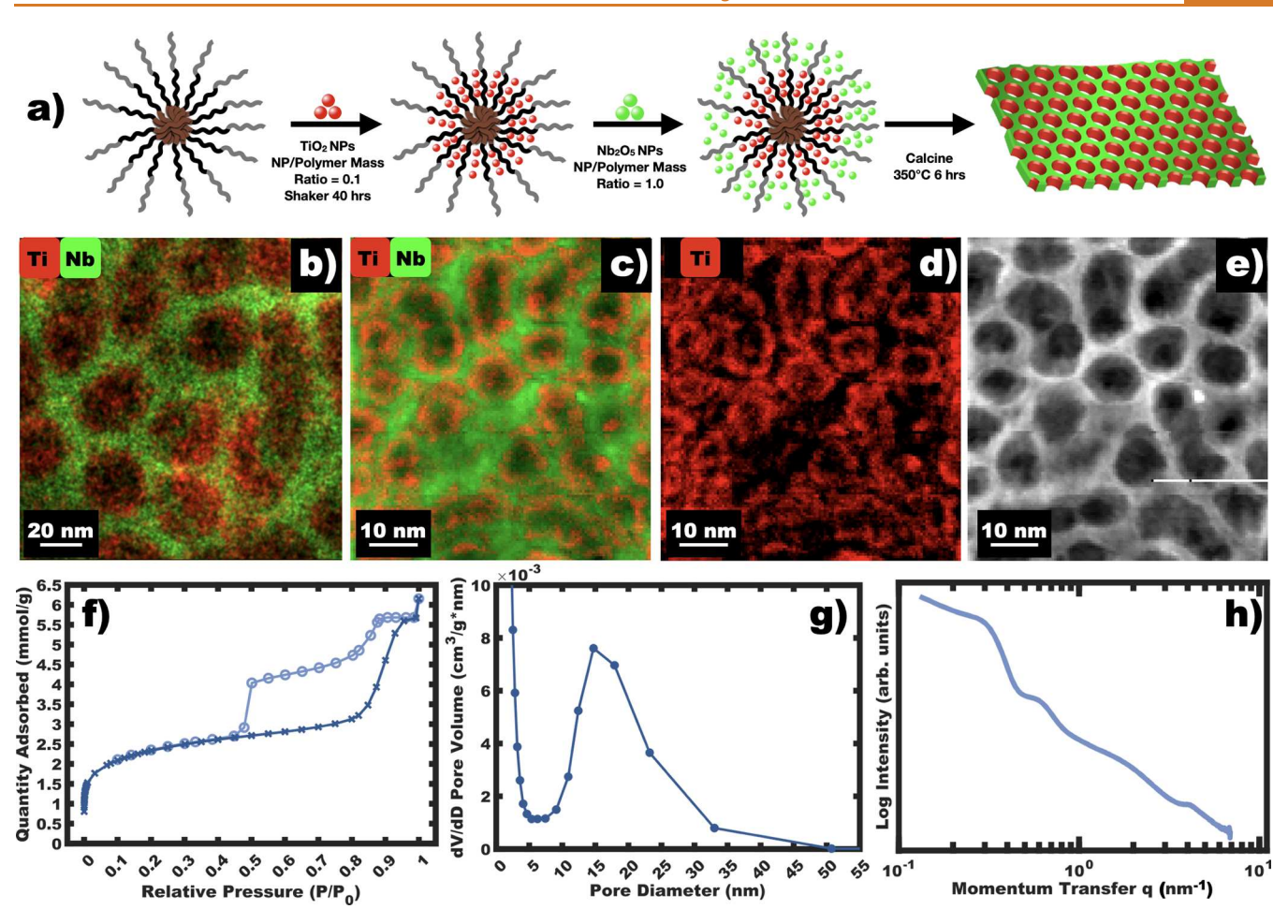


Figure 5. Combining all three design rules enabled uniform porous heterostructure synthesis. The schematic process for PD- TiO_2 – Nb_2O_5 (PCHMA-b-PMMPA-b-PPEGMA) used a hold time to enable NP_1 to permeate through PPEGMA and react with PMMPA (a). Sequence-controlled heterostructures were confirmed with composition maps both (b, STEM-EDS) as-made and (c,d, STEM-EELS) after calcination. The continuous porosity was apparent in images (e, HAADF STEM) as well as by nitrogen physisorption analysis (f, g). The uniform porosity with short-range ordering was also confirmed by SAXS (h).

tinuous porosity that is important for many applications. The formation of interconnected pores was hypothesized to require (sub)saturated SDAs, where corona-corona interactions yield closely packed micelles. This requirement, however, is incompatible with layered heterostructure synthesis, unless an additional dynamically interacting region is added to the SDA. Thus, a triblock terpolymer employing a bis-hydrophilic strategy with both persistent and dynamic regions was designed to enable continuous porosity while retaining sequence-based heterostructure control. The third block added included a PEO-like brush to maintain dynamic NP interactions at the periphery of the micelle template. The poly(cyclohexyl methacrylate-b-methacryloyloxy phosphonic acid-b-poly(ethylene glycol) methacrylate) (PCHMA-b-PMMPA-b-PPEGMA) was prepared using RAFT and postsynthetic modifications (Figures S5-S16 and Table S2). This triblock polymer design significantly improved pore uniformity observed in SEM images of calcined samples (Figure 4b), consistent with the noted hypothesis. This result establishes our second design rule, where a bis-interacting SDA enables interconnected porosity via micelle close packing. Regardless of these two design rules, initial trials with dual NP loading followed by STEM-EDS measurements revealed the mixing of NP₁ and NP₂ (Figures 4c, S17). It was hypothesized that additional time is required with this SDA design due to

competing interactions with PPEGMA slowing the NP₁ reaction with PMMPA. To test this hypothesis, a series of TEM, SEM, and BET experiments (see SI NP Incorporation Experiments) revealed that 40 h of agitation was sufficient for NP₁ to diffuse into PMMPA and react as evidenced by NPs diffusing further into micelles with correspondingly decreasing pore sizes (Figure S18-S19). S2 Considering the relatively rapid loading of NPs into P-NP₁-NP₂ samples, the slow incorporation here suggests a preference for initial NP₁ binding near the PMMPA/PEGMA interface which slows further NP incorporation (reduced free-volume). Please note that this explanation is consistent with well-known immobilization of organics to oxides via even a single phosphonic acid group. This data established the third design rule, where this bis-interacting strategy requires appropriate processing time to enable covalent attachment of NP₁. Thus, a total of three design rules were elaborated to combine heterostructure control with uniform porosity.

Ordered Mesoporous Heterostructure Synthesis. All three design rules were combined in sample PD-TiO₂–Nb₂O₅, where the SDA contained both PMMPA and PEGMA, and where the processing conditions included time to resolve NP₁ incorporation prior to the addition of NP₂ (Figure 5a). The corresponding STEM-EDS measurements of PD-TiO₂–Nb₂O₅ confirmed heterostructure formation (Figure 5b). STEM

electron energy loss spectroscopy (EELS) composition mapping confirmed that this heterostructure was preserved through calcination (PD-TiO₂-Nb₂O₅-calcined) to yield a porous heterostructure of porosity/ TiO_2/Nb_2O_5 with 2.1 \pm 0.4 nm TiO₂ shell thickness (Figure 5c,d). STEM high-angle annular dark-field (HAADF) images revealed the interconnected porosity (Figure 5e). An analogous 3D bulk sample was prepared to examine the interconnected character of the porosity with nitrogen physisorption isotherms. Here BET analysis indicated a high specific surface area of 189 m²/g and BJH analysis indicated a nominal ~15 nm pore diameter (Figure 5f,g). The physisorption isotherm was consistent with type IV with a H₂ hysteresis loop, indicating ink-bottle constrictions between mesopores. Lastly, SAXS measurements of PD-TiO₂-Nb₂O₅-calcined exhibited structure factor peaks consistent with randomly packed spheres having uniform spacing with short-range ordering (Figure 5h).60 Here, the first SAXS peak d-spacing of 20 nm closely matched 19.6 \pm 1.9 nm pore-to-pore spacing measured with the corresponding SEM images (Figure S19). While the STEM data confirms heterostructure preservation after calcination and the BET data confirms polymer removal, the further study of heterointerface sharpness after different crystallization treatments is outside the scope of this study. It is noteworthy that a single reaction vessel was used here from micelle formation through calcination to yield a precision, porous heterostructure. This highlights how the simple elegance of natural self-assembly can lead to the formation of architecturally complex materials with appropriate SDA processing using the three elaborated design rules.

CONCLUSIONS

SDA block polymers were developed that used a repeating motif for persistent SDA-NP interactions to enable one-pot self-assembly of layered porous heterostructures (design rule 1). These persistent interactions were enabled by phosphonic acid groups, which were shown by NMR and dispersion stability experiments to result in robust attachment to metal oxide surfaces. The resulting NP₁-loaded micelles were combined with a second NP2 population to enable the direct synthesis of heterostructures with diverse materials and sequences (P-TiO₂-Nb₂O₅, P-Nb₂O₅-ZrO₂, P-ZrO₂-Nb₂O₅, and P-ZrO₂-TiO₂). Next, interconnected and periodic porosity was shown to benefit from the addition of an additional corona block with dynamic SDA-NP interactions (design rule 2). The competitive binding of the two blocks that interact with NPs (dynamic and persistent) was addressed with an extended agitation process for NP₁ to fully react with the phosphonic acid groups before the addition of NP₂ (design rule 3). The developed approach used a bis-hydrophilic SDA design and appropriately matched processing considerations to enable the self-assembly of mesoporous heterostructures. This elegant combination of these three design rules enables a onepot strategy for self-assembled materials, where the synthetic sequence is encoded into the resulting heterostructure with uniform porosity.

METHODS

The materials, syntheses, and characterization methods are described in detail in the Supporting Information and are briefly summarized here. PS-b-PEO was prepared using ATRP.³⁷ DEPMMA monomer was synthesized by esterification. PCHMA-b-PDEPMMA was prepared using RAFT.⁵⁸ PCHMA-b-PMAA-b-PPEGMA was prepared

using RAFT and was subsequently modified by esterification to yield PCHMA-b-PDEPMMA-b-PPEGMA. The noted PDEPMMA containing block polymers were hydrolyzed using the Mckenna reaction to yield the corresponding phosphonic acid containing PMMPA block.⁵⁸ Micelles were prepared by dissolving polymers in good solvents, followed by the addition of selective solvents and evaporative removal of good solvents. TiO2, Nb2O5, and ZrO2 NPs were prepared from the respective alkoxides under acidic conditions. Binding experiments were carried out by combining micelles with TiO₂ NPs, followed by the addition of base to induce oxide precipitation. The P-NP₁-NP₂ samples were prepared by adding NP₁ to PCHMAb-PMMPA micelles with a 5 min wait before adding NP₂. Sample PD-TiO2-Nb2O5 was prepared by adding TiO2 NPs to PCHMA-b-PMMPA-b-PPEGMA micelles with 40 h of shaking before the addition of Nb₂O₅ NPs. DLS, NMR, TEM, STEM, SEM, BET, and SAXS were used to characterize samples.

ASSOCIATED CONTENT

5 Supporting Information

The Supporting Information is available free of charge at https://pubs.acs.org/doi/10.1021/acsnano.4c01855.

An earlier version of this manuscript is available as a preprint. Materials used, polymer synthesis methods, micelle preparation methods, micelle—NP experiments, DLS, NMR, TEM, STEM, and BET data along with synthesis schemes, tabulated values, and discussion of NP incorporation experiments (PDF)

AUTHOR INFORMATION

Corresponding Author

Morgan Stefik — Department of Chemistry and Biochemistry, University of South Carolina, Columbia, South Carolina 29208, United States; ⊚ orcid.org/0000-0002-2645-7442; Email: morgan@stefikgroup.com

Authors

Taylor Larison – Department of Chemistry and Biochemistry, University of South Carolina, Columbia, South Carolina 29208, United States; orcid.org/0000-0002-4418-9330

Eric R. Williams – Department of Chemistry and Biochemistry, University of South Carolina, Columbia, South Carolina 29208, United States

Mason Wright – Department of Chemistry and Biochemistry, University of South Carolina, Columbia, South Carolina 29208, United States

Mengxue Zhang — Department of Chemistry and Biochemistry, University of South Carolina, Columbia, South Carolina 29208, United States; ◎ orcid.org/0000-0001-6848-314X

John Tengco – Department of Chemical Engineering, University of South Carolina, Columbia, South Carolina 29208, United States; orcid.org/0000-0002-3582-3766

Matthew G. Boebinger – Center for Nanophase Materials Science, Oak Ridge National Laboratories, Oak Ridge, Tennessee 37830, United States; orcid.org/0000-0001-9622-2043

Chuanbing Tang — Department of Chemistry and Biochemistry, University of South Carolina, Columbia, South Carolina 29208, United States; ⊚ orcid.org/0000-0002-0242-8241

Complete contact information is available at: https://pubs.acs.org/10.1021/acsnano.4c01855

Notes

The authors declare no competing financial interest.

ACKNOWLEDGMENTS

T. Larison, E. Williams, M. Zhang, and M. Stefik acknowledge support by the NSF CAREER program, NSF Award No. DMR-1752615. Several STEM imaging and EDS characterization experiments were conducted at the Center for Nanophase Materials Sciences (CNMS), which is a US Department of Energy (DOE), Office of Science User Facility under Award CNMS2023-R-01970. This work was performed in part at the Analytical Instrument Facility (AIF) at North Carolina State University, which is supported by the State of North Carolina and the National Science Foundation (award number ECCS-2025064). The AIF is a member of the North Carolina Research Triangle Nanotechnology Network (RTNN), a site in the National Nanotechnology Coordinated Infastructure (NNCI). This work made use of the South Carolina SAXS Collaborative (SCSC). T. Larison acknowledges Cameron Centers for his artwork contributions.

REFERENCES

- (1) Itoh, K.; Bockris, J. O. Stacked Thin-film Photoelectrode Using Iron Oxide. *J. Appl. Phys.* **1984**, *56*, 874–876.
- (2) Lauhon, L. J.; Gudiksen, M. S.; Wang, D.; Lieber, C. M. Epitaxial Core—Shell and Core—Multishell Nanowire Heterostructures. *Nature* **2002**, *420*, 57–61.
- (3) Zhang, J.; Tang, Y.; Lee, K.; Ouyang, M. Nonepitaxial Growth of Hybrid Core-Shell Nanostructures with Large Lattice Mismatches. *Science* **2010**, 327, 1634–1638.
- (4) Mulla, R.; Dunnill, C. W. Core—Shell Nanostructures for Better Thermoelectrics. *Mater. Adv.* **2022**, *3*, 125–141.
- (5) Kartini, I.; Menzies, D.; Blake, D.; Da Costa, J. C. D.; Meredith, P.; Riches, J. D.; Lu, G. Q. Hydrothermal Seeded Synthesis of Mesoporous Titania for Application in Dye-Sensitised Solar Cells (DSSCs). J. Mater. Chem. 2004, 14, 2917–2921.
- (6) Zukalovà, M.; Zukal, A.; Kavan, L.; Nazeeruddin, M. K.; Liska, P.; Grätzel, M. Organized Mesoporous TiO2 Films Exhibiting Greatly Enhanced Performance in Dye-Sensitized Solar Cells. *Nano Lett.* **2005**, *5*, 1789–1792.
- (7) Peter, L. M. Dye-Sensitized Nanocrystalline Solar Cells. *Phys. Chem. Chem. Phys.* **2007**, *9*, 2630–2642.
- (8) Jiao, F.; Shaju, K. M.; Bruce, P. G. Synthesis of Nanowire and Mesoporous Low-Temperature LiCoO2 by a Post-Templating Reaction. *Angew. Chem.* **2005**, *117*, 6708–6711.
- (9) Liu, H.; Bi, Z.; Sun, X. G.; Unocic, R. R.; Paranthaman, M. P.; Dai, S.; Brown, G. M. Mesoporous TiO2-B Microspheres with Superior Rate Performance for Lithium Ion Batteries. *Adv. Mater.* **2011**, 23, 3450–3454.
- (10) Li, X.; Gu, M.; Hu, S.; Kennard, R.; Yan, P.; Chen, X.; Wang, C.; Sailor, M. J.; Zhang, J.-G.; Liu, J. Mesoporous Silicon Sponge as an Anti-Pulverization Structure for High-Performance Lithium-Ion Battery Anodes. *Nat. Commun.* **2014**, *5*, No. 4105.
- (11) Carbon, C.; Korenblit, Y.; Rose, M.; Kockrick, E.; Borchardt, L.; Kvit, A.; Kaskel, S.; Yushin, G. High-Rate Electrochemical Capacitors. *ACS Nano* **2010**, *4*, 1337–1344, DOI: 10.1021/nn901825y.
- (12) Zhu, Y.; Murali, S.; Stoller, M. D.; Ganesh, K. J.; Cai, W.; Ferreira, P. J.; Pirkle, A.; Wallace, R. M.; Cychosz, K. A.; Thommes, M.; Su, D.; Stach, E. A.; Ruoff, R. S. Carbon-Based Supercapacitors. *Science* **2011**, 332, 1537–1541.
- (13) Jiang, H.; Ma, J.; Li, C. Mesoporous Carbon Incorporated Metal Oxide Nanomaterials as Supercapacitor Electrodes. *Adv. Mater.* **2012**, *24*, 4197–4202.
- (14) Augustyn, V.; Come, J.; Lowe, M. A.; Kim, J. W.; Taberna, P. L.; Tolbert, S. H.; Abruña, H. D.; Simon, P.; Dunn, B. High-Rate

- Electrochemical Energy Storage through Li + Intercalation Pseudocapacitance. *Nat. Mater.* **2013**, *12*, 518–522.
- (15) Chang, H.; Joo, S. H.; Pak, C. Synthesis and Characterization of Mesoporous Carbon for Fuel Cell Applications. *J. Mater. Chem.* **2007**, *17*, 3078–3088.
- (16) Ye, Y.; Jo, C.; Jeong, I.; Lee, J. Functional Mesoporous Materials for Energy Applications: Solar Cells, Fuel Cells, and Batteries. *Nanoscale* **2013**, *5*, 4584–4605.
- (17) Xiao, J.; Cheng, K.; Xie, X.; Wang, M.; Xing, S.; Liu, Y.; Hartman, T.; Fu, D.; Bossers, K.; van Huis, M. A.; van Blaaderen, A.; Wang, Y.; Weckhuysen, B. M. Tandem Catalysis with Double-Shelled Hollow Spheres. *Nat. Mater.* **2022**, *21*, 572–579.
- (18) Navrotsky, A. Energetic Clues to Pathways to Biomineralization: Precursors, Clusters, and Nanoparticles. *Proc. Natl. Acad. Sci. U. S. A.* **2004**, *101*, 12096–12101.
- (19) Kamat, S.; Su, X.; Ballarini, R.; Heuer, A. H. Structural Basis for the Fracture Toughness of the Shell of the Conch Strombus Gigas. *Nature* **2000**, *405*, 1036–1040.
- (20) Hwang, H. Y.; Iwasa, Y.; Kawasaki, M.; Keimer, B.; Nagaosa, N.; Tokura, Y. Emergent Phenomena at Oxide Interfaces. *Nat. Mater.* **2012**, *11*, 103–113.
- (21) Stefik, M.; Cornuz, M.; Mathews, N.; Hisatomi, T.; Mhaisalkar, S.; Grätzel, M. Transparent, Conducting Nb:SnO 2 for Host–Guest Photoelectrochemistry. *Nano Lett.* **2012**, *12*, 5431–5435.
- (22) Mannhart, J.; Schlom, D. G. Oxide Interfaces—An Opportunity for Electronics. *Science* **2010**, 327, 1607–1611.
- (23) Huang, Z.; Ariando; Wang, X. R.; Rusydi, A.; Chen, J.; Yang, H.; Venkatesan, T. Interface Engineering and Emergent Phenomena in Oxide Heterostructures. *Adv. Mater.* **2018**, *30*, No. 1802439, DOI: 10.1002/adma.201802439.
- (24) Dey, S.; Fan, C.; Gothelf, K. V.; Li, J.; Lin, C.; Liu, L.; Liu, N.; Nijenhuis, M. A. D.; Saccà, B.; Simmel, F. C.; Yan, H.; Zhan, P. DNA Origami. *Nat. Rev. Methods Prim.* **2021**, *1*, No. 13, DOI: 10.29172/562c76d9-02eb-4582-9d33-536bc9402994.
- (25) Zhao, D.; Feng, J.; Huo, Q.; Melosh, N.; Fredrickson, G. H.; Chmelka, B. F.; Stucky, G. D. Triblock Copolymer Syntheses of Mesoporous Silica with Periodic 50 to 300 Angstrom Pores. *Science* **1998**, 279, 548–552, DOI: 10.1126/science.279.5350.548.
- (26) Zhao, T.; Elzatahry, A.; Li, X.; Zhao, D. Single-Micelle-Directed Synthesis of Mesoporous Materials. *Nat. Rev. Mater.* **2019**, *4*, 775–791.
- (27) Lee, J.; Christopher Orilall, M.; Warren, S. C.; Kamperman, M.; Disalvo, F. J.; Wiesner, U. Direct Access to Thermally Stable and Highly Crystalline Mesoporous Transition-Metal Oxides with Uniform Pores. *Nat. Mater.* **2008**, *7*, 222–228.
- (28) Lokupitiya, H. N.; Stefik, M. Cavitation-Enabled Rapid and Tunable Evolution of High-: Xn Micelles as Templates for Ordered Mesoporous Oxides. *Nanoscale* **2017**, *9*, 1393–1397.
- (29) van den Bergh, W.; Williams, E. R.; Vest, N. A.; Chiang, P.-H.; Stefik, M. Mesoporous TiO 2 Microparticles with Tailored Surfaces, Pores, Walls, and Particle Dimensions Using Persistent Micelle Templates. *Langmuir* **2021**, *37*, 12874–12886.
- (30) van den Bergh, W.; Larison, T.; Fornerod, M. J. J.; Guldin, S.; Stefik, M. Faster Intercalation Pseudocapacitance Enabled by Adjustable Amorphous Titania Where Tunable Isomorphic Architectures Reveal Accelerated Lithium Diffusivity. *Batteries Supercaps* 2022, 5, No. e202200122, DOI: 10.1002/batt.202200122.
- (31) Suchomski, C.; Reitz, C.; Sousa, C. T.; Araujo, J. P.; Brezesinski, T. Room Temperature Magnetic Rare-Earth Iron Garnet Thin Films with Ordered Mesoporous Structure. *Chem. Mater.* **2013**, 25, 2527–2537.
- (32) Brezesinski, K.; Wang, J.; Haetge, J.; Reitz, C.; Steinmueller, S. O.; Tolbert, S. H.; Smarsly, B. M.; Dunn, B.; Brezesinski, T. Pseudocapacitive Contributions to Charge Storage in Highly Ordered Mesoporous Group v Transition Metal Oxides with Iso-Oriented Layered Nanocrystalline Domains. *J. Am. Chem. Soc.* **2010**, *132*, 6982–6990.
- (33) Yao, Y.; Metwalli, E.; Moulin, J.-F.; Su, B.; Opel, M.; Müller-Buschbaum, P. Self-Assembly of Diblock Copolymer—Maghemite

- Nanoparticle Hybrid Thin Films. ACS Appl. Mater. Interfaces 2014, 6, 18152–18162.
- (34) Mayeda, M. K.; Hayat, J.; Epps, T. H.; Lauterbach, J. Metal Oxide Arrays from Block Copolymer Thin Film Templates. *J. Mater. Chem. A* **2015**, 3, 7822–7829.
- (35) Liang, C.; Hong, K.; Guiochon, G. A.; Mays, J. W.; Dai, S. Synthesis of a Large-Scale Highly Ordered Porous Carbon Film by Self-Assembly of Block Copolymers. *Angew. Chem., Int. Ed.* **2004**, 43, 5785–5789.
- (36) Deng, Y.; Liu, C.; Gu, D.; Yu, T.; Tu, B.; Zhao, D. Thick Wall Mesoporous Carbons with a Large Pore Structure Templated from a Weakly Hydrophobic PEO-PMMA Diblock Copolymer. *J. Mater. Chem.* **2008**, *18*, 91–97.
- (37) Williams, E. R.; McMahon, P. L.; Reynolds, J. E.; Snider, J. L.; Stavila, V.; Allendorf, M. D.; Stefik, M. Tailored Porous Carbons Enabled by Persistent Micelles with Glassy Cores. *Mater. Adv.* **2021**, 2, 5381–5395.
- (38) Warren, S. C.; Messina, L. C.; Slaughter, L. S.; Kamperman, M.; Zhou, Q.; Gruner, S. M.; DiSalvo, F. J.; Wiesner, U. Ordered Mesoporous Materials from Metal Nanoparticle-Block Copolymer Self-Assembly. *Science* **2008**, 320, 1748–1752.
- (39) Yao, L.; Lin, Y.; Watkins, J. J. Ultrahigh Loading of Nanoparticles into Ordered Block Copolymer Composites. *Macromolecules* **2014**, 47, 1844–1849.
- (40) Liu, R.; Shi, Y.; Wan, Y.; Meng, Y.; Zhang, F.; Gu, D.; Chen, Z.; Tu, B.; Zhao, D. Triconstituent Co-Assembly to Ordered Mesostructured Polymer–Silica and Carbon–Silica Nanocomposites and Large-Pore Mesoporous Carbons with High Surface Areas. *J. Am. Chem. Soc.* **2006**, *128*, 11652–11662.
- (41) Chu, H.; Yu, C.; Wan, Y.; Zhao, D. Synthesis of Ordered Mesoporous Bifunctional TiO2-SiO2-Polymer Nanocomposites. *J. Mater. Chem.* **2009**, *19*, 8610.
- (42) Duan, L.; Hung, C.; Wang, J.; Wang, C.; Ma, B.; Zhang, W.; Ma, Y.; Zhao, Z.; Yang, C.; Zhao, T.; Peng, L.; Liu, D.; Zhao, D.; Li, W. Synthesis of Fully Exposed Single-Atom-Layer Metal Clusters on 2D Ordered Mesoporous TiO2 Nanosheets. *Angew. Chem., Int. Ed.* **2022**, *61*, No. e202211307, DOI: 10.1002/anie.202211307.
- (43) Chiu, J. J.; Kim, B. J.; Kramer, E. J.; Pine, D. J. Control of Nanoparticle Location in Block Copolymers. *J. Am. Chem. Soc.* **2005**, 127 (14), 5036–5037.
- (44) Lin, Y.; Boker, A.; He, J.; Sill, K.; Xiang, H.; Abetz, C.; Li, X.; Wang, J.; Emrick, T.; Long, S.; Wang, Q.; Balazs, A.; Russell, T. P. Self-Directed Self-Assembly of Nanoparticle/Copolymer Mixtures 2005, 434 (7029), 55–59.
- (45) Zubarev, E. R.; Xu, J.; Sayyad, A.; Gibson, J. D. Amphiphilicity-Driven Organization of Nanoparticles into Discrete Assemblies. *J. Am. Chem. Soc.* **2006**, 128 (47), 15098–15099.
- (46) Kim, B. J.; Fredrickson, G. H.; Kramer, E. J. Effect of Polymer Ligand Molecular Weight on Polymer-Coated Nanoparticle Location in Block Copolymers. *Macromolecules* **2008**, *41* (2), 436–447.
- (47) de Villiers, M. M.; Otto, D. P.; Strydom, S. J.; Lvov, Y. M. Introduction to Nanocoatings Produced by Layer-by-Layer (LbL) Self-Assembly. *Adv. Drug Deliv. Rev.* **2011**, *63* (9), 701–715.
- (48) Mai, Y.; Eisenberg, A. Controlled Incorporation of Particles into the Central Portion of Block Copolymer Rods and Micelles. *Macromolecules* **2011**, 44 (8), 3179–3183.
- (49) Fuertes, M. C.; López-Alcaraz, F. J.; Marchi, M. C.; Troiani, H. E.; Luca, V.; Míguez, H.; Soler-Illia, G. J. A. A. Photonic Crystals from Ordered Mesoporous Thin-Film Functional Building Blocks. *Adv. Funct. Mater.* 2007, *17*, 1247–1254.
- (50) Zeininger, L.; Portilla, L.; Halik, M.; Hirsch, A. Quantitative Determination and Comparison of the Surface Binding of Phosphonic Acid, Carboxylic Acid, and Catechol Ligands on TiO₂ Nanoparticles. *Chem. A Eur. J.* **2016**, 22 (38), 13506–13512.
- (51) Guerrero, G.; Mutin, P. H.; Vioux, A. Anchoring of Phosphonate and Phosphinate Coupling Molecules on Titania Particles. *Chem. Mater.* **2001**, *13*, 4367–4373.

- (52) Sevrain, C. M.; Berchel, M.; Couthon, H.; Jaffres, P.-A. Phosphonic Acid: Preparation and Applications. *Beilstein J. Org. Chem.* **2017**, *13*, 2186–2213.
- (53) Owen, J. S.; Park, J.; Trudeau, P. E.; Alivisatos, A. P. Reaction Chemistry and Ligand Exchange at Cadmium-Selenide Nanocrystal Surfaces. *J. Am. Chem. Soc.* **2008**, *130*, 12279–12281.
- (54) Clearfield, A. Recent Advances in Metal Phosphonate Chemistry II. Curr. Opin. Solid State Mater. Sci. 2002, 6, 495–506.
- (55) Rivas, B. L.; Pereira, E.; Gallegos, P.; Homper, D.; Geckeler, K. E. Metal Ion Binding Capability of the Water-Soluble Poly(Vinyl Phosphonic Acid) for Mono-, Di-, and Trivalent Cations. *J. Appl. Polym. Sci.* **2004**, *92*, 2917–2922.
- (56) Prabakaran, M.; Venkatesh, M.; Ramesh, S.; Periasamy, V. Corrosion Inhibition Behavior of Propyl Phosphonic Acid—Zn2+System for Carbon Steel in Aqueous Solution. *Appl. Surf. Sci.* **2013**, 276, 592–603.
- (57) Gomes, R.; Hassinen, A.; Szczygiel, A.; Zhao, Q.; Vantomme, A.; Martins, J. C.; Hens, Z. Binding of Phosphonic Acids to CdSe Quantum Dots: A Solution NMR Study. *J. Phys. Chem. Lett.* **2011**, *2*, 145–152.
- (58) Larison, T.; Stefik, M. Persistent Micelle Corona Chemistry Enables Constant Micelle Core Size with Independent Control of Functionality and Polyelectrolyte Response. *Langmuir* **2021**, *37*, 9817–9825.
- (59) Sarkar, A.; Stefik, M. How to Make Persistent Micelle Templates in 24 h and Know It Using X-Ray Scattering. *J. Mater. Chem. A* **2017**, *5*, 11840–11853.
- (60) Wang, X.; Dormidontova, E. E.; Lodge, T. P. The Order-Disorder Transition and the Disordered Micelle Regime for Poly(Ethylenepropylene-b-Dimethylsiloxane) Spheres. *Macromolecules* **2002**, *35*, 9687–9697.
- (61) Stefik, M.; Larison, T.; Williams, E.; Wright, M.; Tengco, J. M.; Boebinger, M.; Tang, C.; Research Square. One-Pot Synthesis of Sequence-Controlled Mesoporous Heterostructures. 2024 DOI: 10.21203/rs.3.rs-3470490/v1.